Microtubule as Nanobioelectronic Nonlinear Circuit*

Dalibor L. Sekulić[1], Miljko V. Satarić[1]

Abstract: In recent years, the use of biological molecules has offered exciting alternatives to conventional synthetic methods. Specific methods use various biological templates to direct the deposition and patterning of inorganic materials. Here we have established a new electrical model of microtubules as a biological nanoscale circuit based on polyelectrolyte features of cylindrical biopolymers. Our working hypothesis is that microtubules play an active role in sub-cellular computation and signaling via electronic and protonic conductivity and can thus be made useful in hybrid materials that offer novel electronic characteristics. We verify these hypotheses both computationally and analytically through a quantitative model based on the atomic resolution structures of the key functional proteins.

Keywords: Nanobioelectronics, Microtubule, Protein, Nano pore, Nonlinear circuit.

1   Introduction

Nanobioelectronics is a thriving new area of research at the interface between the life sciences and nanotechnology, which deals with structures of dimensions ranging from 1 nm to 100 nm, below the range of lithographic fabrication techniques [1]. Nanobiotechnology aims to exploit biomolecules and the processes carried out by them for the development of novel functional materials and devices [2] and, more speculatively, nanomachines, perhaps nanorobots. These developments open up an exciting possibility of building integrated systems in which electronic and biomolecular components function side–by–side. Biopolymer structures are attractive as templates to form nanoscale architectures for electronics because of their size, geometry and ability to interact with inorganic materials.

Proteins represent fertile territory for nanobioelectronics because they have properties ideal for engineering purposes. They possess sophisticated architectures at nanoscale dimensions, rich chemistry and versatile enzymatic

---

[1]Faculty of Technical Sciences, University of Novi Sad, Trg Dositeja Obradovića 6, 21000 Novi Sad, Serbia; E-mails: dalsek@uns.ac.rs, bomisat@neobee.net.

activities. Proteins are capable of carrying out complex tasks in cells. We need think only of examples such as the linear motors of the cytoskeleton, voltage–gated ion channels, DNA replication complexes, or the photosynthetic reaction centres [2]. By genetic engineering and/or chemical modification or by using proteins in ways not found in nature, nanobiotechnology can harness the power of proteins to create new components for materials and devices.

Most studies in this area have been performed on DNA molecules [3, 4]. It has been shown that DNA may be used as a template to form silver nanowires connecting gold electrodes [5]. Microtubules (MTs) comprise another interesting type of protein structure that may be a good candidate for designing and manufacturing electronic nanodevices. MTs are cytoskeletal biopolymers shaped as nanotubes. *In vivo* MT cylinders have 13 protofilaments (PFs), as shown in Fig. 1a. The external and internal diameters of MTs are 25 and 15 nm, and the length can reach up to 10–15 μm in a cell. The dimensions of a constituent tubulin dimer (TD) are $(4{\times}4{\times}8)$ nm^3, and there are 13 dimers from 13 PFs considered as an elementary ring of MT. An important point is that every tubulin has a long thin flexible tail (TT) protruding out from the MT cylinder (every dimer has two TT). These TTs have an important role in electric capacitance in our model, as shown Fig. 1b.
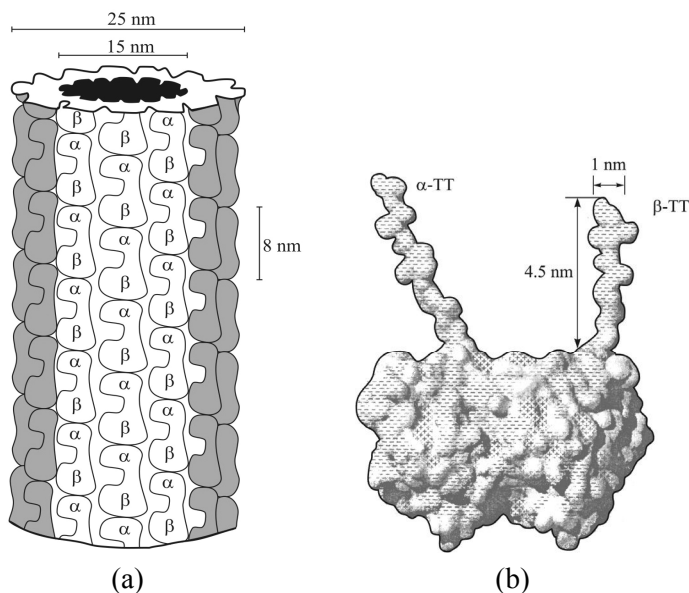

Fig. 1 – (a) *A MT hollow cylinder of* 13 *parallel PFs with denoted characteristic dimensions: outer and inner diameters of* 25 nm *and* 15 nm*, respectively, and TD length of* 8 nm; (b) *The topology of a* TD *with* TT*s whose dimensions are: the length of* 4.5 nm *and diameter of* 1 nm*.*

In this paper, we explained the polyelectrolyte character of MT and described the basic components of the MT as a biomolecular nanoscale nonlinear electronic circuit. Then we set up an electrical model of the MT using capacitive and resistive components. Also, we analytically and numerically analyzed the voltage equation.

2   Characterization of the Electric Components of MT

In as much MTs are mostly negatively charged on their outer surface they are true polyelectrolyte polymers. This is the consequence of the fact that numerous amino acids forming tubulin have many negatively charged residues under physiological conditions. As a result, every MT attracts positive counter ions close to its surface creating so called ionic cloud (IC), while negative ions of cytosol are repelled such that a cylindrical depletion area is created around the MT. The width of this depleted layer is called the Bjerrum length, l_B, defined by equating the Coulomb attraction energy of the ions with the thermal energy:

$$e^2 / \left(4\pi\varepsilon_0\varepsilon l_B\right) = k_B T. \tag{1}$$

Taking $e = 1.6\times10^{-19}$ C, $\varepsilon_0 = 8.85\times10^{-12}$ F/m, $\varepsilon = 80$ (for cytosol) and $k_B = 1.38\times10^{-23}$ J/K, for the physiological temperature $T = 310$ K we obtain $l_B = 0.67$ nm. The occurrence of Manning condensation around the polymer of radius r also depends on the fact that the salt concentration n in the cytosol should be low enough to satisfy the inequality $l_{Db} \gg r$, where the Debye length, $l_{Db,}$ is defined by

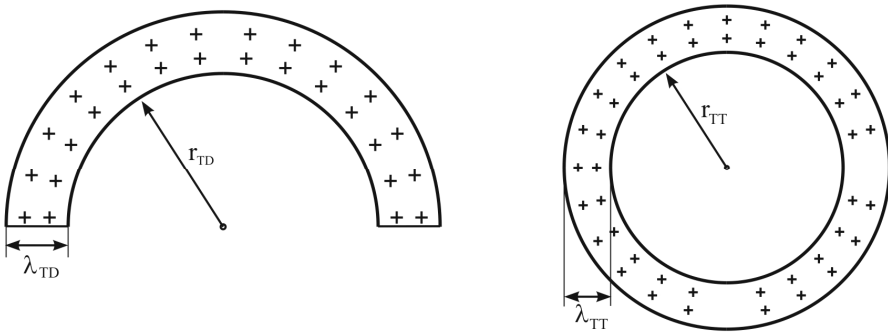$$l_{Db}^{-1} = \left(8\pi n l_B\right)^{1/2}. \tag{2}$$

Fig. 2 – *Schematic representation of the counter–ion charge distributions surrounding a* TD (*left panel*) *and a* TT (*right panel*).

Since the radius of a TT is of the order of 0.5 nm and the radius of a TD is of the order of 2.5 nm, while the Debye length for the cytosol is of the order of 10 nm [6], we see that the condition in (2) holds for both radii. Thus, we are now able to reliably estimate the respective condensate thickness λ:

$$\lambda = A\left(rl_{Db}\right)^{1/2}, \quad A < 1, \tag{3}$$

where A depends only weakly on the Manning parameter q_0. Taking $A = 1/2$ one finds the corresponding values for the TD (λ_{TD}) and TT (λ_{TT}) as follows: $\lambda_{TD} = 2.5$ nm; $\lambda_{TT} = 1.1$ nm. These values will be used in our calculations of the corresponding capacity and resistivity, see Fig. 2.

2.1 The capacitance of an elementary unit of MT

In an earlier paper [7], a detailed Poisson-Boltzmann approach was used to evaluate the capacitance of an elementary ring of an MT which consists of 13 dimers. Here, we adopt the same expression which reads:

$$C_0 = \frac{2\pi\varepsilon_0\varepsilon l}{\ln\left(1 + \dfrac{l_B}{R_{IC}}\right)}, \tag{4}$$

where l stands for the length of a polymer unit and $R_{IC} = r_{TD} + \lambda_{TT}$ for the outer radius of an IC. The other parameters have already been introduced. We first estimate the elementary unit of each MT protofilament (EUP) capacitance contributed by a TD, see Fig. 3. With $l_{TD} = 8$ nm and $R_{IC} = r_{TD} + \lambda_{TT} = 5$ nm, we find for TD (including only the outer surface) $C_{TD} = 1.4\times10^{-16}$ F. Analogously, we can consider an extended TT as a smaller cylinder with the radius $r_{TT} = 0.5$ nm and the thickness of its IC equal to $\lambda_{TT} = 1$ nm. Its extended effective length should be $l_{TT}^{eff} = 4.5\,\text{nm} - 2.5\,\text{nm} = 2\,\text{nm}$ meaning that its part close to the tubulin surface is already embedded. Thus, we now estimate the corresponding capacitance, $C_{TT} = 0.26\times10^{-16}$ F. Accounting for the fact that two TTs are present in each tubulin dimer, we finally obtain $2\times C_{TT} = 0.52\times10^{-16}$ F. The two capacitance values above are considered to correspond to a parallel arrangement with respect to each other, so that the total maximal capacitance of an EUP is readily estimated as:

$$C_0 = C_{TD} + 2\times C_{TT} = 1.92\times10^{-16}\,\text{F}. \tag{5}$$

We have emphasized that TTs capacitance must change with an increasing concentration of condensed cations due to the shrinking of flexible TTs. These changes are slightly different due to the different structures of α and β type TTs. To include this case we introduce the reduced factor of nonlinearity as follows

$$b_0 = \frac{b_\alpha b_\beta}{b_\alpha + b_\beta}, \tag{6}$$

where b_α and b_β stand for the respective TTs. This implies that the charge of an EUP capacitor diminishes with an increased voltage in a nonlinear way $\Delta C_0 = C_0 b_0 v$, $b_0 v \ll 1$.
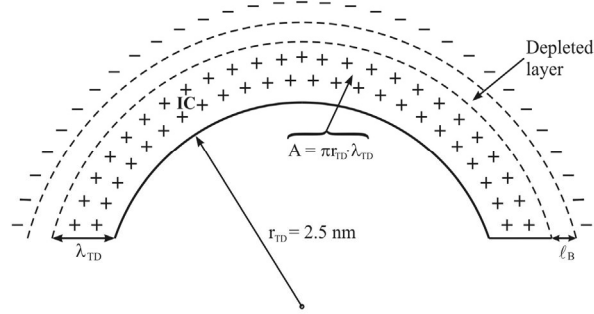

Fig. 3 – *Schematic illustration of the calculation of the MT capacitance.*

Additionally, we account for the tilting movements of TTs under the combined action of thermal fluctuations [8] and a changing voltage due to an incoming ionic wave. Thus, the part of EUP capacitance contributed by TTs should also change by TTs tilt as shown in Fig. 4. The change of the effective length of a TT is an additional factor affecting the capacitance, ΔC_{TT}. We assume that this change can be adequately described by the oscillating function

$$\Delta l_{TT}^{eff} = l_{TT}^{eff} \sin\left[\Omega(t - t_0)\right] \cong l_{TT}^{eff} \Omega(t - t_0). \tag{7}$$
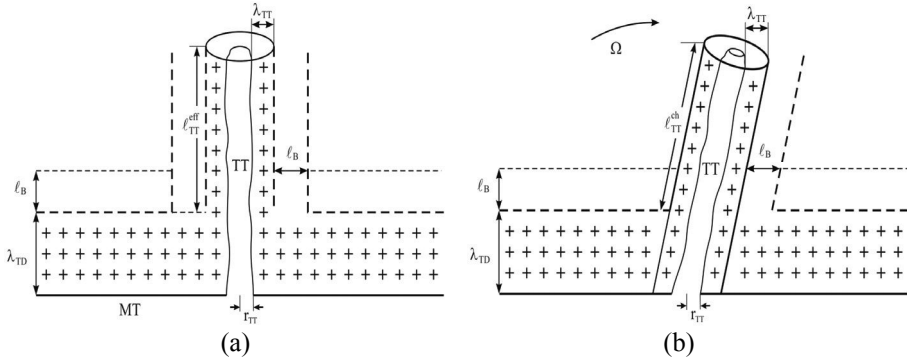

Fig. 4 – *A comparison between*: (a) *an extended* TT; (b) *a tilting* TT *due to oscillations.*

So that the capacitance changes linearly with a change in the effective TTs length

$$\Delta C_{TT} = C_0 \Gamma_0 \Omega(t - t_0), \tag{8}$$

where the frequency Ω is much lower than the inverse charging time of the EUP capacitor due to the strong viscous damping of the TT tilt, thus justifying the

linearization of the above sine function in (7). In some sense, this effect is similar in character to the thermal ratchet mechanism combined with an asymmetric ionic potential. Including the two aspects of TTs dynamics described above, the charge of EUP can be expressed as follows

$$Q = C_0 \left[1 - \Gamma_0 \Omega(t - t_0) - b_0 v \right] v, \tag{9}$$

where Γ_0 is a dimensionless parameter.

2.2 The conductance of Nano–pores

Between neighboring PFs there are two distinct types of (NPs). NP–1, see Fig. 5 left, is located where an inter–dimer β/α interface of one TD lies next to the inter–dimer β/α interface of the adjacent TD molecule. The so–called NP–2 arises where an intra–dimer interface of one dimer lies next to the intra–dimer interface of an adjacent TD of a neighboring PF, see Fig. 5 right. Freedman et al [8] used HOLE and AMBER programs to estimate the effective radius of the narrowest points within these NPs and found them to be 0.4 nm and 0.47 nm for type–1 and type–2 NPs, respectively.
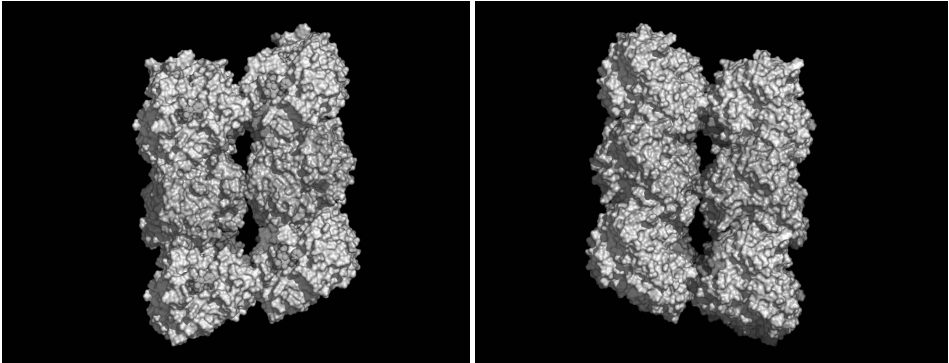

Fig. 5 – *An illustration of the NPs in the A and B MT lattices, respectively.*

Based on the modified version of the Poisson–Boltzmann equation, the conductances of NPs are determined in terms of Brownian dynamics of ions. For the type–1 NP, inner and outer cationic conductances were calculated to be 2.93 nS and 1.22 nS, respectively, while for type–2 NP the respective values of 7.80 nS and 4.98 nS were found.

Finally, we could include the conductance of both NPs to account for the leakage of IC cations into the lumen area. Thus we have

$$G_0 = \sigma_1 + \sigma_2 = (2.93 + 7.8)\text{nS} = 10.7\,\text{nS}. \tag{10}$$

It is expected that NPs exert greater resistance than the volume of IC around EUP.

2.3 The resistance of an elementary unit of MT

Regarding the ohmic resistance, if we ignore ionic current leaks through the depleted layer, the dominant current flows in parallel with the MT axis charging EUP capacitors and partly leaking through NPs. The resistance attributed to this kind of ionic flow can be estimated on the basis of experimental evidence provided by the electro–orientation method performed on MTs *in vitro* [6]. Taking the reported measured value of MT ionic conductivity as $\sigma = (0.15 \pm 0.01)$ Sm^{-1}, and adopting a simplifying assumption that the resistivity within an IC patch beyond an EUP is homogeneous, the resistance of an EUP with the length $l = 8$ nm and the cross–sectional area $A = \pi r_{TD}\lambda_{TD}$, $A = 19.625$ nm^2, see Fig. 3, is estimated as:

$$R_0 = \frac{1}{\sigma}\frac{l}{A} = 2.7 \times 10^9 \, \Omega \; . \tag{11}$$

This is obviously an extremely high value of resistance which is most likely an over–estimate. We therefore prefer the computed resistance shown in Table 3 of reference [8], referred to as the outer sheath–outer sheath resistance for complete 13 PFs, namely $R_{13} = 4.75 \times 10^6 \, \Omega$. The resistance for our EUP will be 13 times greater, i.e.,

$$R_0 = 13R_{13} = 6.2 \times 10^7 \, \Omega \; . \tag{12}$$

This value appears to be more consistent with the resistance of two NPs which follows from (10).

2.4 The inductance of an elementary unit of MT

The straightforward calculation performed in [9] revealed that the order of magnitude of the inductance of an elementary ring in MT is of the order of $L \sim 10{-}15$ H. This is very small value regarding pertaining reactive resistance. For example, if the frequency is of the order of MHz we have $\omega L \sim 10{-}9 \, \Omega$ for inductive impedance, while capacitive impedance amounts $(\omega C){-}1 \sim 109 \, \Omega$. Similar discrepancy holds for the energies of corresponding fields

$$\frac{1}{2}Li^2 \ll \frac{1}{2}C_0 v^2, \tag{13}$$

since i is of the order of nA and v of the order of several mV. Thus, the role of inductance in this model could be safely ignored.

3   The Model of MT as Nonlinear Circuit

On the basis of above estimations for the resistive components of the MT we are now in the position to establish the corresponding model of MT as nonlinear nanoscale circuit. A typical section scheme is shown in Fig. 6. Applying Kirchhoff's low to ladder of ERs, we have:

$$i_n - i_{n+1} = \frac{\partial Q_n}{\partial t} + G_0 v_n, \qquad v_{n-1} - v_n = R_0 i_n \; . \tag{14}$$

Introducing the characteristic impedance of our system $Z = 1/(C_0 \omega)$ and establishing new function $u(x, t)$, $u_n = Z^{1/2} i_n = Z^{1/2} v_n$, we can safely expand u_n in a continuum approximation using a Taylor series in terms of a small spatial parameter l (the length of a dimer). Then using the travelling–wave form of the function $u(x, t)$ with dimensionless space and time variables (ξ, τ), we get the following voltage equation

$$\left(\frac{ZC_0 s}{T_0} - 2 \right) \frac{\partial u}{\partial \tau} + \frac{1}{3} \frac{\partial^3 u}{\partial \xi^3} + ZC_0 \Gamma_0 \Omega (\xi - \xi_0) \frac{\partial u}{\partial \xi} +$$
$$+ 2 \frac{Z^{3/2} b_0 C_0 s}{T_0} u \frac{\partial u}{\partial \xi} + \left(ZG_0 + Z^{-1} R_0 - ZC_0 \Gamma_0 \Omega \right) u = 0. \tag{15}$$

Here, $T_0 = R_0 C_0$ is the characteristic charging (discharging) time of an EUP capacitor C_0 through the resistance R_0 and $v_0 = l/T_0$ is the characteristic velocity of spreading the ionic wave. The dimensionless speed, space and time variables are chosen to be respectively:

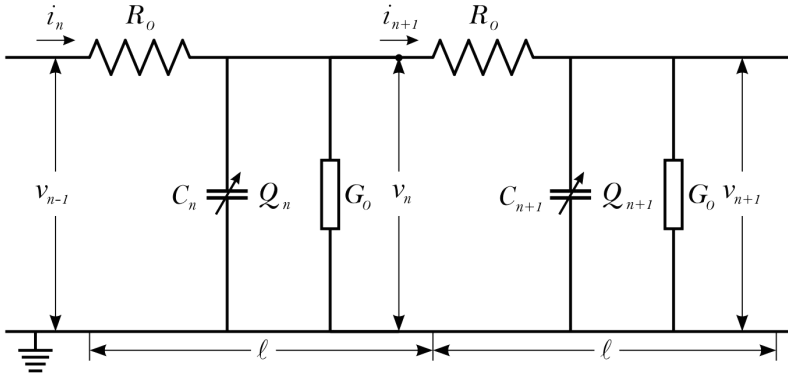$$s = \frac{v}{v_0} \leq 1, \quad \xi = \frac{x}{l} - \tau, \quad \tau = s \frac{t}{T_0} \; . \tag{16}$$

Fig. 6 – *An effective circuit diagram for the n-th* ER *with characteristic elements for Kirchhoff's laws.*

4 Analisis of the Voltage Equation

Imposing that the condition

$$\frac{ZC_0 s}{T_0} > 2 \tag{17}$$

holds, we then estimate the characteristic impedance of EUP as $Z = 1.24 \times 10^8\,\Omega$ for $s = 1$. For $s = 1$ one obtains the cutoff frequency $\omega_{max} = 4.3 \times 10^7\,\text{s}^{-1}$ or $f_{max} = 6.8 \times 10^6$ Hz. This indicates that the characteristic frequency matches the order of magnitude of frequency Ω which describes the TTs oscillations. We now establish the compact form of (15) as:

$$\frac{\partial u}{\partial \tau} + \beta \frac{\partial^3 u}{\partial \xi^3} + \alpha u \frac{\partial u}{\partial \xi} + \gamma(\xi)\frac{\partial u}{\partial \xi} + \delta u = 0, \tag{18}$$

where the abbreviations were introduced as follows:

$$\alpha = \frac{2Z^{3/2}b_0 C_0 s}{T_0\left(\dfrac{ZC_0 s}{T_0} - 2\right)}, \quad \beta = \frac{1}{3\left(\dfrac{ZC_0 s}{T_0} - 2\right)},$$

$$\delta = \frac{ZG_0 + Z^{-1}R_0 - ZC_0\Gamma_0\Omega}{\left(\dfrac{ZC_0 s}{T_0} - 2\right)}, \quad \gamma(\xi) = \frac{ZC_0\Gamma_0\Omega(\xi - \xi_0)}{\left(\dfrac{ZC_0 s}{T_0} - 2\right)} = \gamma_0\left(\xi - \xi_0\right). \tag{19}$$

The detailed procedure of solving (18) is given in [10], so that the function $u(\xi, \tau)$ has the following form:

$$u\left(\xi, \tau\right) = u_0 \exp\left(-2\gamma_0\tau\right)\cosh^{-2}\left\{\left[\frac{\alpha u_0}{4\beta}\exp(-2\gamma_0\tau)\right]^{1/2} \cdot\right.$$

$$\left. \cdot\left[\xi - \xi_0\left(1 - \exp\left(\gamma_0\tau\right)\right) + \frac{\alpha u_0}{3\beta}\left(1 - \exp\left(3\gamma_0\tau\right)\right)\exp\left(-2\gamma_0\tau\right)\right]\right\}. \tag{20}$$

If we use the set of estimated and chosen parameters, we readily see that all dimensionless parameters (19) lie between zero and one ($\beta = 0.33$, $\gamma_0 = 0.17$, $\delta = 0.34$) staying within the same order of magnitude. This suggests that we should inspect numerically the behaviour of the solution of (18) when the parameters α, β, γ_0 and ξ_0 take slightly different values which are done next. Analysing the set of plots in Fig. 7 we can see the competition between nonlinearity α and the dispersion β, as well as the role of inhomogeneity γ_0. In the case represented in Fig. 7b we have balanced all parameters. The soliton solution preserves its width but its amplitude decays rather rapidly so that over the length of about $500\,l$ it becomes negligible. The above view shows the deceleration of the soliton solution along its path. Fig. 7c shows the case with increased nonlinearity ($\alpha = 0.5$). It is remarkable that it exhibits not only a higher localization but also a slower decay of its amplitude. The advantage of this case lies in the fact that the velocity of the soliton solution decreases very slightly.
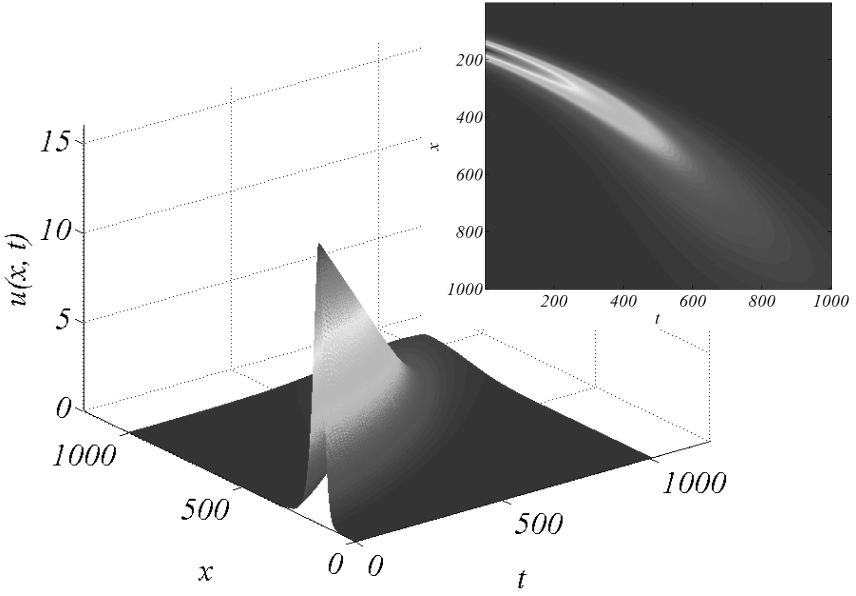
(a)
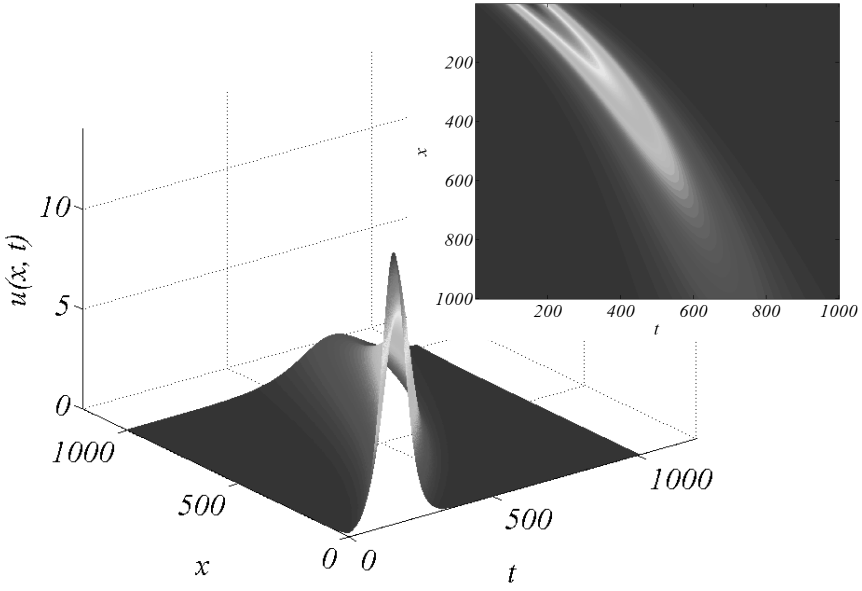
(b)

Fig. 7 – *Numerical solutions of u(x, t) for:*
(a) $\alpha = 0.2$, $\beta = 0.33$, $\gamma_0 = 0.17$, $\xi_0 = 0.1$;
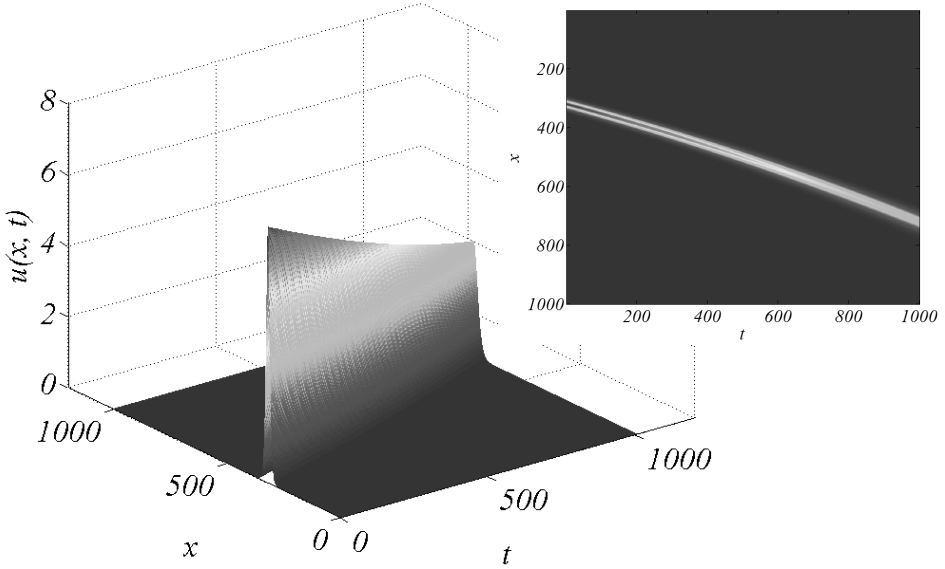(b) $\alpha = 0.1$, $\beta = 0.1$, $\gamma_0 = 0.1$, $\xi_0 = 0.1$.

Fig. 7c – *Numerical solutions of u(x, t) for*: α = 0.5, β = 0.1, γ₀ = 0.1, ξ₀ = 0.1.

We estimate its average velocity as follows:

$$\left.\begin{array}{l}\Delta x \approx 400l = 400 \times 8\text{nm} = 3.2\mu\text{m}, \\ \Delta t = 1000T_0 = 10^3 \times 1.2 \times 10^{-8}\text{s} = 1.2 \times 10^{-5}\text{s}\end{array}\right\} \quad v = \frac{\Delta x}{\Delta t} = 0.26\frac{\text{m}}{\text{s}}.$$

The range of this soliton is 3.2 μm which is of the order of the cell's diameter. Therefore, it appears that the ionic pulse with such parameter values could be efficiently transferred within the cell.

5   Conclusions

In this paper, we theoretically analysed the use of MTs as protein structure for building biomolecular nanoscale nonlinear circuit in the context of the polyelectrolyte character of these cytoskeletal filaments. We have taken into account the role of two aspects of this cylindrical biopolymer, its NPs and very sensitive TTs. Both of them are responsible for the nonlinear character of the overall electrical capacitance of MTs. Our solution, (20), was analyzed numerically for the set of parameters in Fig 7. It is apparent that the solitonic wave loses its energy due to ohmic resistance but it preserves the stable localized form. In the case presented in Fig. 7c with an increased nonlinearity parameter, the solitonic pulse exhibits greater robustness and it progresses with an almost constant velocity and only a slight decay of its initial amplitude. This

117

demonstrates the role of flexible TTs which could be of decisive importance for the stable localized character of ionic pulses along MTs. The order of magnitude of soliton–like localized pulses arising within the scope of our study ranges from mm/s to a several cm/s which are very reasonable values.

In this study, the particular attention was paid to the role of NPs existing between neighboring dimmers within a MT wall which exhibit properties like ionic channels. These NPs are candidates to explain some properties of MTs resembling to unipolar transistors enabling the rectification and amplification of ionic currents.

Finally, the experimental work of Priel et al [11] demonstrated that the electrical signal amplification resulting from the presence of MTs can be directly attributed to nonlinear ionic currents guided by MTs in close similarity to the framework developed by our present model. In fact, these measurements inspired the authors to consider the role MTs can play as biotransistors taking part in cognitive processes which is another interesting application of nonlinear ionic conductance of MTs.

6   Acknowledgments

7   References

[1]   C.R. Lowe: Nanobiotechnology: The Fabrication and Applications of Chemical and Biological Nanostructure, Current Opinion in Structural Biology, Vol. 10, No. 4, Aug. 2000, pp. 428 – 434.

[2]   Y. Astier, H. Bayley, S. Howorka: Protein Components for Nanodevices, Current Opinion in Chemical Biology, Vol. 9, No. 6, Dec. 2005, pp. 576 – 584.

[3]   V.D. Lakhno, V.B. Sultanov: On the Possibility of Electronic DNA Nanobiochips, Journal of Chemical Theory and Computation, Vol. 3, No. 3, May 2007, pp. 703 – 705.

[4]   V.D. Lakhno: DNA Nanobioelectronics, International Journal of Quantum Chemistry, Vol. 108, No. 11, April 2008, pp. 1970 – 1981.

[5]   E. Braun, Y. Eichen, U. Sivan, G. Ben–Yoseph: DNA–templated Assembly and Electrode Attachment of a Conducting Silver Wire, Nature, Vol. 391, No. 6669, Febr. 1998, pp. 775 – 778.

[6]   I. Minoura, E. Muto: Dielectric Measurement of Individual Microtubules using the Electro Orientation Method, Biophysical Journal, Vol. 90, No. 10, May 2006, pp. 3739 – 3748.

[7]   M.V. Satarić, D.L. Sekulić, M.V. Živanov: Solitonic Ionic Currents along Microtubules, Journal of Computational and Theoretical Nanoscience, Vol. 7, No. 11, Nov. 2010, pp. 2281 – 2290.

[8]   H. Freedman, V. Rezania, A. Priel, E. Carpenter, S.Y. Noskov, J.A. Tuszynski: Model of Ionic Currents through Microtubule Nanopores and the Lumen, Physical Review E, Vol. 81, No. 5, May 2010, pp. 051912.

[9] M.V. Satarić., D.I. Ilić, N.M. Ralević, J.A. Tuszynski: A Nonlinear Model of Ionic Wave Propagation along Microtubules, European Biophysics Journal, Vol. 38, No. 5, June 2009, pp. 637 – 647.

[10] D.L. Sekulić, B.M. Satarić, J.A. Tuszynski, M.V Satarić: Nonlinear Ionic Pulses along Microtubules, European Physical Journal E: Soft Matter, Vol. 34, No. 5, May 2011, Art. no. 49.

[11] A. Priel, A.J. Ramos, J.A. Tuszynski, H.F. Contiello: A Biopolymer Transistor: Electrical Amplification by Microtubules, Biophysical Journal, Vol. 90, No. 12, June 2006, pp. 4639 – 4643.